JOURNAL OF MECHANICS OF CONTINUA AND MATHEMATICAL SCIENCES
www.journalimcms.org

ISSN (Online) : 2454 -7190 Vol.-21, No.-08, August (2026) pp 138-155 ISSN (Print) 0973-8975

ANALYSIS OF TRANSIENT RADIATIVE MHD BIOCONVECTION FLOW OF Fe_3O_4–MOS_2 HYBRID NANOFLUID OVER A RAMPED INCLINED OSCILLATING PLATE IN A ROTATING POROUS MEDIUM WITH MASS TRANSFER

Prabakaran V.[1] , S. Senthamilselvi[2]

[1,2]Department of Mathematics, Vels Institute of Science, Technology & Advanced Studies, Chennai-600117, Tamil Nadu, India.

Email: [1]Prabakaran1202@gmail.com, [2]msselvi2305@gmail.com

Corresponding Author: **S. Senthamilselvi**

https://doi.org/10.26782/jmcms.2026.08.00009

(Received: May 08, 2026; Revised: July 30, 2026; Accepted: August 14, 2026)

Abstract

The transient radiative magnetohydrodynamic bioconvective flow of an Fe_3O_4-MoS_2 hybrid nanofluid over a ramped, inclined, oscillating plate in a rotating porous medium is investigated numerically in this work. The model mathematically integrates the effects of heat and mass transfer, thermal radiation, rotation, porous permeability, and motile microbes. Using appropriate similarity transformations, governing equations for momentum, temperature, nanoparticle concentration, or microbe density are converted into the non-dimensional equations. The coupled system is then solved using the Crank-Nicolson finite-difference approach. The impact of several significant parameters, including Peclet number, magnetic parameter, bioconvection Lewis number, or radiation parameter, on the flow characteristics is investigated numerically. This establishes that fluid velocity increases as the Peclet number increases, but with higher bioconvection values. The Lewis number reduces the velocity profile. Temperature as well as concentration profiles Radiation and diffusion parameters significantly impact temperature and concentration profiles. by radiation and diffusion parameters.

Keywords: Hybrid nanofluid; Bioconvection; porous medium; Thermal radiation; Oscillating plate; Crank Nicolson.

I. Introduction

Nanofluids have received substantial interest due to their better heat transfer capability compared to traditional base fluids. When nanoparticles are added to a host fluid, the thermal conductivity increases significantly, as does the overall efficiency of thermal systems for many engineering and industrial applications. Hybrid nanofluids are a complex type of working fluid discovered recently. These fluids contain two different species of nanoparticles, for instance, Fe_3O_4 and MoS_2, which have better thermal performance, stability, and heat transmission characteristics than single-component nanofluids. Besides the temperature effects, the stability and transport characteristics of these fluids are strongly affected by the bioconvection due to motile bacteria. Density gradients produced by the collective motion of microorganisms have a significant impact on flow dynamics or improve the transfer of mass or heat. Thermo-diffusion (Dufour) or Hall current combined impacts on MHD flow of dense, non-compressible, conducting fluid transferring fluid passing through an exponentially vertical permeable plate were investigated by Bijjula Prabhakar Ready in XXII. XV solved the same problem without the Hall current. Later, he studied the unstable motion of responding and emitting conducting substances by electricity on a surface slipping in a hydro magnetic boundary layer with his colleague XIV and IV oscillation and Newtonian heating, which causes motion that is time-dependent and enhances heat transmission. Prasun Choudhary and his co-workers have investigated several aspects of nanofluid flow throughout many configurations. In V, the authors explored the behavior of -Al_2O_3-water nanofluid on a magnetic flat plate and evaluated it numerically. Also, VI studied nonlinear, stretchable, porous, and gyrotactic microorganisms. They stressed the role of bioconvection mechanisms. In IX, the authors studied the thermal behavior and density distribution of motile bacteria in nano(tiny)flow. Apart from X, the authors explored “MHD tetra-hybrid nanofluid flow” with velocity slip and demonstrated the advantages of deploying several nanoparticles to enhance the thermal efficiency. Furthermore, in VII, a hybrid nanofluid model based on the mass centre with thermal radiation was developed to study the characteristics of heat transmission in wedge geometries. Finally, in VIII, the study discovered that bioconvection (microorganisms' effects) influences the stability of flow, the concentration distribution, and rates of microbe or mass transfer.

The impact of rotational motion or thermal radiation on parabolic fluid flow was examined by Dilip Jose et al. XXVI. The behavior of Casson fluid in parabolic geometries was examined by Selvaraj et al. XVII. Later, they XVI extended their study to rotating porous media with “variable mass diffusion.” Furthermore, the Dufour effect and Hall current effects were incorporated in XIV to enhance the understanding of interconnected transport phenomena. Lakshmikaanth et al. XII indicated that fluid velocity escalates with heat generation and Hall current, whereas it diminishes due to thermal radiation. This study was subsequently expanded in XIII to incorporate thermo-diffusion effects. Kavitha and Selvaraj XI noted that the Coriolis force impedes fluid velocity, but the Dufour effect amplifies temperature distribution. Radha et al. XXIII investigated MHD impacts on the flow of Casson fluid adjacent to a parabolic accelerated vertical plate having thermal diffusion. The flow across a plate with exponential acceleration has been studied by Selvaraj and Jothi XXIV, taking internal heat generation into consideration. Rajkumar et al. Selvaraj et al. XXV studied Hall and Dufour Effects on MHD flow over a parabolically accelerated vertical plate.XVIII, XIX examined the magnetohydrodynamic free convection flow of Casson fluid across oscillating porous plates, considering viscous dissipation, the Dufour effect, and ion-slip current in both vertical and inclined configurations, incorporating Hall current effects. Rao et al., XX addressed the governing equations employing the Keller-box approach and showed that both radiation and magnetic factors greatly affect the thickness of the thermal boundary layer, whereas hybrid nanofluids have enhanced thermal performance relative to mono nanofluids. Almarashi et al. III demonstrated that while the Bejan number, or local Nusselt number, decreases as the magnetic parameter elevates, temperature, entropy generation, and skin friction significantly increase. Flow stability and thermal transfer efficiency were examined by Asaigeethan et al. XI in association with Casson fluid properties and magnetic effects. Aboel-Magd et al. I studied the dynamics of the microorganisms on a rotating disc, considering the thermal radiation and the activation energy. Vijayaragavan et al. XXVII tried to figure out how to theoretically solve the problem of heat as well as mass transfer within MHD Casson fluid flow past a sloped porous plate while Dufour and chemical reactions were taking place. By analyzing a Fe_3O_4-MoS_2 hybrid nanofluid's transient MHD bioconvection flow over a ramped, inclined, oscillating plate in a rotating porous medium, this study fills a gap in the literature. This work is unique in that it incorporates hybrid nanofluid characteristics, motile microbes, and radiative heat transfer all within a single transient framework. Moreover, the employment of an unconditionally stable Crank-Nicolson finite difference scheme guarantees uniqueness and existence of a solution to the controlling non-dimensional system, thereby facilitating accurate and consistent computation of the coupled nonlinear equations.

II. Mathematical Formulation

The unstable motion of an electrically conducting, viscous, and incompressible fluid across a non-conducting vertical plate at z = 0 is studied in this study. The z-direction is taken into the fluid region normal to the plate, whereas the x-direction is taken along the slant surface of the plate. A uniform transverse magnetic field B_0 is present when the conducting fluid flows. The plate and fluid are at rest with a constant ambient temperature T'_∞ and concentration C'_∞ for $t' \leq 0$. For t' >0, the temperature and concentration of the plate are suddenly raised to constant values C'_w and T'_w, respectively, while the plate oscillates at velocity $u'=u_0\cos wt$. "Governing equations" for transient flow are derived employing these assumptions.

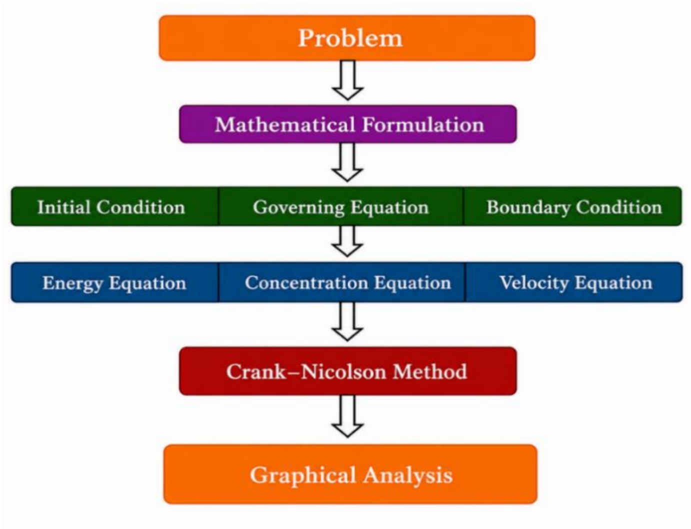

Fig. 1. Flowchart of the problem

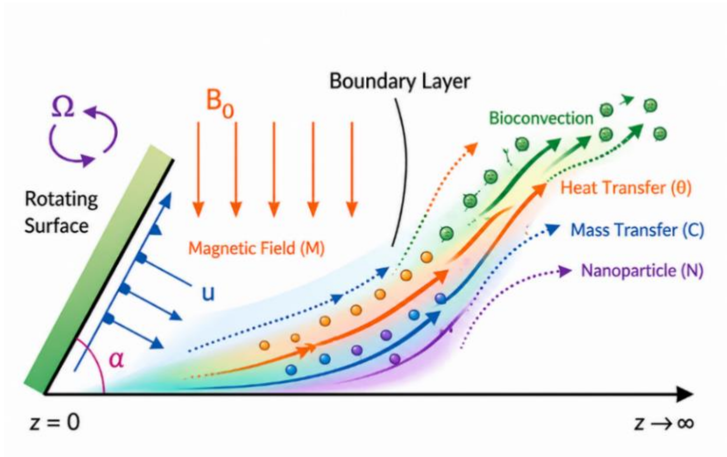

Fig. 1. Schematic of physical model

Consider an incompressible hybrid nanofluid containing motile microorganisms that flows past an inclined, oscillating plate through a rotating porous medium under a transverse magnetic field.

$$q = (u', v', 0) \;\; B = (0,0,B_0),\, \Omega = (0,0,\Omega)$$

$$\nabla . q = 0 \tag{1}$$

$$\rho hnf\left[\frac{\partial q}{\partial t'} + (q.\nabla)q + 2\Omega \times q\right] = -\nabla . p + \mu hnf\, \nabla q + \rho g + J \times B - \frac{\mu hnf}{K} q \tag{2}$$

By using the Boussinesq Approximation

For a transverse magnetic field

$$J \times B = -\sigma hnf\, B_0^2\, u'$$

Hence, the Coupled Momentum equations are

$$\rho hnf \frac{\partial u'}{\partial t'} = \mu hnf \frac{\partial^2 u'}{\partial z'^2} - \sigma hnf B_0^2 u' - \frac{\mu hnf}{K} u' + \rho hnf g \cos\alpha \left[\, \beta_T (T' - T'_\infty) + \beta_C (C' - C'_\infty) + \beta_N (N' - N'_\infty)\right] - 2\rho hnf \Omega v' \tag{3}$$

$$\rho hnf \frac{\partial v'}{\partial t'} = \mu hnf \frac{\partial^2 v'}{\partial z'^2} - \sigma hnf B_0^2 v' - \frac{\mu hnf}{K} v' + 2\rho hnf \Omega u' \tag{4}$$

$$(\rho c_p) hnf \frac{\partial T'}{\partial t'} = k_{hnf} \frac{\partial^2 T'}{\partial z'^2} \left(\frac{3k^* + 16\sigma^* T'^3_\infty}{3k^*}\right) + Q_0 (T' - T'_\infty) \tag{5}$$

$$\frac{\partial C'}{\partial t'} = Dhnf \frac{\partial^2 C'}{\partial z'^2} - K_r (C' - C'_\infty) \tag{6}$$

$$\frac{\partial N'}{\partial t'} = D_n \frac{\partial^2 N'}{\partial z'^2} - W_C \frac{\partial}{\partial z'} \left(N' \frac{\partial C'}{\partial z'}\right) \tag{7}$$

Using

$$u' = 0 = v', T' - T'_\infty = 0, C' - C'_\infty = 0, N' = N'_\infty \;\; \forall \;\; z' \geq 0, t' \leq 0$$
$$u' = u_0 \cos(wt'), T' = T'_\infty - \frac{t'}{t_0}(-T'_w + T'_\infty),$$
$$C' = C'_\infty - \frac{t'}{t_0}(-C'_w + C'_\infty),$$
$$N' = N'_\infty - \frac{t'}{t_0}(-N'_w + N'_\infty) \;\; for \; 0 < t' \leq t_0 \tag{8}$$
$$T' = T'_w, \;\; C' = C'_w, N' = N'_w \;\; \text{for} \;\; t' \geq 0$$
$$u' \to 0, v' \to 0, \;\; T' \to T'_\infty, \;\; C' \to C'_\infty, N' \to N'_\infty$$
$$\text{as} \;\; z' \to \infty \text{ and } \; t' \geq 0$$

Rosseland approximation is used for the local radiant [19],

$$\frac{\partial q'_r}{\partial y'} = -4a^*\sigma^* (T'^4_\infty - T'^4) \tag{9}$$

$$T'^4 \cong T'^3_\infty(-3T'_\infty + 4T') \tag{10}$$

Substitute the eqs. (5) and (6) in eqs (3) reduces to

$$\rho C_p \frac{\partial T'}{\partial t'} = k\frac{\partial^2 T'}{\partial y^2} + 16a^*\sigma(T'_\infty - T')T'^3_\infty \tag{12}$$

The subsequent dimensionless quantities

$$U = \frac{u'}{u_0}, \;\; V = \frac{v'}{u_0}, t = \frac{t'U_0}{L}, \;\; z = z'\frac{1}{L}, \theta = \frac{T' - T'_\infty}{T'_w - T'_\infty}$$
$$C = \frac{C' - C'_\infty}{C'_w - C'_\infty}, Gr = \frac{g\beta_T(T'_w - T'_\infty)L}{u_0^2}, \phi = \frac{N' - N'_\infty}{N'_w - N'_\infty}, Gc = \frac{g\beta_C(C'_w - C'_\infty)L}{u_0^2}$$
$$, Gn = \frac{g\beta_N(N'_w - N'_\infty)l}{u_0^2} \;\; M = \frac{\sigma_{hnf}B_0^2L^2}{v_{hnf}\rho_{hnf}}, Pr = \frac{v_{hnf}(\rho c_p)_{hnf}}{k_{hnf}}, K_0 = \tag{13}$$
$$\Omega = \frac{\Omega' L^2}{v_{hnf}}, w = \frac{wv}{u_0^2}, Sc = \frac{v_{hnf}}{D_{hnf}}, Rd = \frac{16\sigma^* T'^3_\infty}{3k^* k_{hnf}}, Q = \frac{Q' vL^2}{\rho c_p u_0^2}, K = \frac{K_C L^2}{v_{hnf}}$$

$$Pe = \frac{Wc(C'_w - C'_\infty)L^2}{v_{hnf}}, Lb = \frac{v_{hnf}}{Dn},$$

Using (13) in the eqs. (3) to (6), we have derived

$$\frac{\partial u}{\partial t} = \frac{\partial^2 u}{\partial z^2} - Mu - K_0 u + Gr\cos\alpha\,\theta + Gc\cos\alpha\,C + Gn\cos\alpha x - 2\Omega v \tag{14}$$
$$\frac{\partial u}{\partial t} = \frac{\partial^2 u}{\partial z^2} - Mv - K_0 v + 2\Omega u \tag{15}$$
$$\frac{\partial \theta}{\partial t} = \frac{(1+Rd)}{P_r}\frac{\partial^2 \theta}{\partial z^2} + Q\theta \tag{16}$$
$$\frac{\partial C}{\partial t} = \frac{1}{S_c}\frac{\partial^2 C}{\partial z^2} - KC \tag{17}$$
$$\frac{\partial \phi}{\partial t} = \frac{1}{Lb}\frac{\partial^2 \phi}{\partial z^2} - Pe\frac{\partial}{\partial z}\left(\phi\frac{\partial C}{\partial z}\right) \tag{18}$$

By employing boundary condition (20) alongside equations (14) and (15), we can now consolidate the complex velocity, $q = U + iV$, into a singular equation.

$$\frac{\partial q}{\partial t} = \frac{\partial^2 q}{\partial z^2} - (M + K_0 - 2\Omega i)q + Gr\cos\alpha\,\theta + Gc\cos\alpha\,C + Gn\cos\alpha\,\phi \tag{19}$$

The initial and boundary conditions that match are

$$\left.\begin{array}{c} q = C = \theta = \phi = 0 \text{ when } t \leq 0, z \geq 0 \\ q = coswt,\ \theta = \phi = 1, C = t, y = 0 \text{ and } t > 0 \\ q \to 0, \theta \to 0, \phi \to 0 \text{ and } C \to 0 \text{ as } z \to \infty \end{array}\right\} \tag{20}$$

III. Solution

A coupled system of nonlinear partial differential equations is defined through governing eqns. (14-18) and the specified first and boundary conditions. The system's mathematical complexity makes it extremely challenging to discover an exact analytical solution. Consequently, the Crank-Nicolson method is employed to solve equations numerically. Physical domain $0 \leq z \leq z_{max}$z_ is discretised into uniform grid points with spatial step size Δz, while the time domain is divided into equal intervals of length Δt

Let $z_i = i\Delta z$, $i = 0,1,1, \ldots\ldots N$ *and* $t^n = n\Delta t$, $n = 0,1,2, \ldots.$

then $\theta(z_i, t^n) = \theta_i^n$, $C(z_i, t^n) = C_i^n$, $\phi(z_i, t^n) = \phi_i^n$ and $q(z_i, t^n) = q_i^n$

The Crank–Nicolson approach is used to estimate the diffusion terms using the average of spatial derivatives at time levels n or n+1.

$$\frac{\theta_i^{n+1} - \theta_i^n}{\Delta t} = \left(\frac{(\theta_{i-1}^{n+1} - 2\theta_i^{n+1} + \theta_{i+1}^{n+1}) + (\theta_{i-1}^n - 2\theta_i^n + \theta_{i+1}^n)}{2(\Delta z)^2}\right)\frac{(1+R_d)}{P_r} + Q\left(\frac{\theta_i^{n+1} + \theta_i^n}{2}\right) \tag{21}$$

Let $r = \frac{(1+Rd)\nabla t}{2Pr(\Delta z)^2}$ and $s = \frac{Q\Delta t}{2}$ then equation (18) becomes

$$-r\theta_{i-1}^{n+1} + (1 + 2r - s)\theta_i^{n+1} - r\theta_{i+1}^{n+1} = r\theta_{i-1}^n + (1 + 2r - s)\theta_i^n + r\theta_{i+1}^n \tag{22}$$

$$\frac{C_i^{n+1} - C_i^n}{\Delta t} = \frac{1}{Sc}\left(\frac{(C_{i+1}^{n+1} - 2C_i^{n+1} + C_{i-1}^{n+1}) + (C_{i+1}^n - 2C_i^n + C_{i-1}^n)}{2(\Delta z)^2}\right) - K\left(\frac{C_i^{n+1} + C_i^n}{2}\right) \tag{23}$$

Let $a = \frac{\nabla t}{2Sc(\Delta z)^2}$ and $b = \frac{K\Delta t}{2}$ then equation (20) becomes

$$-aC_{i-1}^{n+1} + (1 + 2a + b)C_i^{n+1} - aC_{i-1}^{n+1} = aC_{i-1}^n + (1 - 2a - b)C_i^n + aC_{i+1}^n \tag{24}$$

$$\frac{\Phi_i^{n+1} - \phi_i^n}{\Delta t} = \frac{1}{Lb}\left(\frac{(\phi_{i-1}^{n+1} - 2\phi_i^{n+1} + \phi_{i+1}^{n+1}) + (\phi_{i-1}^n - 2\phi_i^n + \phi_{i+1}^n)}{2(\Delta z)^2}\right)$$

$$-Pe\left(\frac{1}{\Delta z}\right)^2 \begin{bmatrix} \left(\frac{\phi_{i+1}^n}{2}\right)\left(\frac{C_{i+2}^n - C_i^n}{2}\right) \\ -\left(\frac{\phi_i^n}{2}\right)\left(\frac{C_i^n - C_{i-2}^n}{2}\right) \end{bmatrix} \tag{25}$$

Let $r_1 = \frac{\nabla t}{2Lb(\Delta z)^2}$, $D_i = r_1(\phi_{i-1}^n + \phi_{i+1}^n) + (1 - 2r_1)\phi_i^n - \Delta t Pe\left(\frac{\phi_{i+1}^n D_{i+1}^n - \phi_{i-1}^n D_{i1}^n}{2\Delta z}\right)$

and $D_i^n = \frac{C_{i+1}^n - C_{i-1}^n}{2\Delta z}$ then Eqn (22) gives

$$-r_1\phi_{i-1}^{n+1} + (1 + 2r_1)\phi_i^{n+1} - r_1\theta_{i-1}^{n+1} = D_i \tag{26}$$

$$\frac{q_i^{n+1}-q_i^n}{\Delta t} = \left(\frac{(q_{i+1}^{n+1}-2q_i^{n+1}+q_{i-1}^{n+1})+(q_{i+1}^{n}-2q_i^{n}+q_{i-1}^{n})}{2(\Delta z)^2}\right) - m\left(\frac{q_i^{n+1}+q_i^n}{2}\right)$$

$$+Gr\ cos\alpha\ \frac{\theta_i^{n+1}-\theta_i^n}{2\Delta t} + Gc\ cos\alpha \frac{C_i^{n+1}-C_i^n}{2\Delta t} + Gn\ cos\alpha \frac{\phi_i^{n+1}-\phi_i^n}{2\Delta t} \quad (27)$$

Let $r_2 = \frac{\Delta t}{2(\Delta z)^2}$, then Eqn (24) gives

$$-r_2 q_{i-1}^{n+1} + \left(1 + 2r_2 + m\frac{\Delta t}{2}\right) q_i^{n+1} = r_2(q_{i-1}^n + q_{i+1}^n)\left(1 - 2r_2 - m\frac{\Delta t}{2}\right) q_i^n$$

$$+\frac{\Delta t}{2}\left(Gr\ cos\alpha(\theta_i^{n+1} + \theta_i^n) + Gc\ cos\alpha(C_i^{n+1} + C_i^n) + Gn\ cos\alpha(\phi_i^{n+1} + \phi_i^n)\right) \quad (28)$$

where m= $(M + K_0 + 2i\Omega)$ and $K_0 = \frac{1}{k_1}$

IV. Results and Discussion

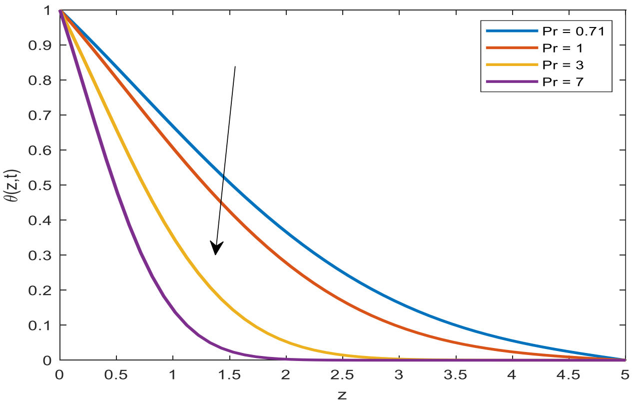

Fig. 2. Temperature for various values of Prandtl number (Pr)

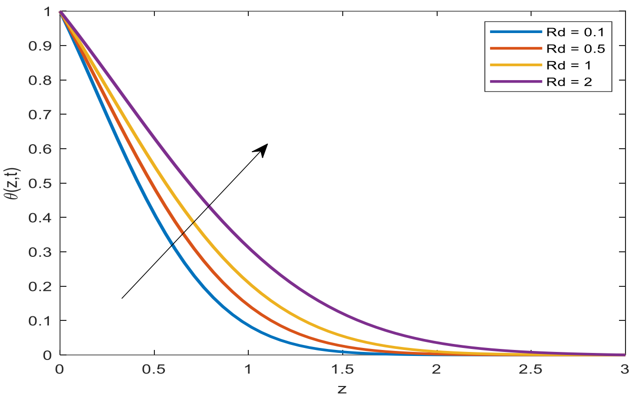

Fig. 3. Temperature distribution for various values of Thermal Radiation(Rd)

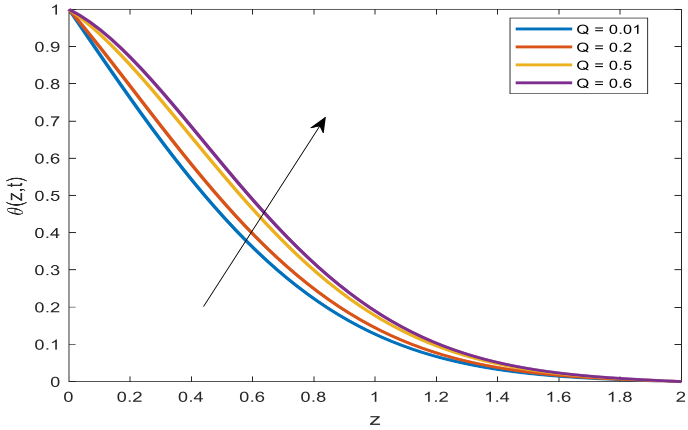

Fig. 4. Temperature distribution for various values of heat generation parameter (Q

The temperature profile in Figure 2 reduces as “Prandtl number (Pr)” increases. This is because a thinner thermal boundary layer results from a decreased thermal diffusivity for higher Pr values, which limits heat penetration into the fluid. Therefore, the rotating porous hybrid nanofluid flow's heat transfer behavior is significantly influenced by the Prandtl number. In Figure 3, “radiation parameter (Rd)” elevates the temperature profile. Temperature increases because of thermal radiation, which provides the fluid with additional energy and encourages heat transmission. Therefore, the radiative effects are significant for the enhancement of thermal transport in the rotating porous hybrid nanofluid system. As the values of the heat-generating parameter (Q) increase, Figure 4 shows that the temperature profile increases significantly. Figure 4 demonstrates how the temperature profile increases significantly as the values of the heat-generating parameter (Q) increase. Findings demonstrated that the heat generation significantly improves the rotating porous hybrid nanofluid flow system's thermal performance.

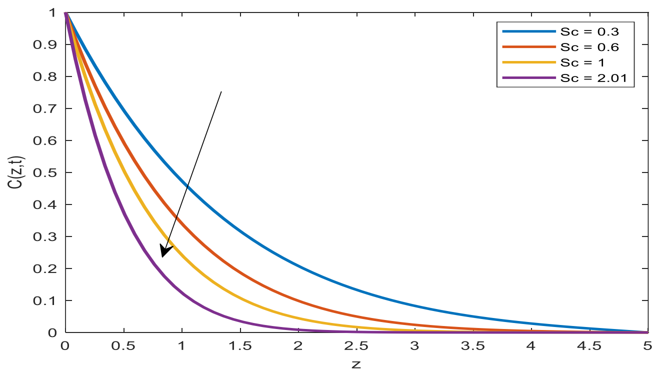

Fig. 5. Concentration distribution for various values of Schmidt number (Sc)

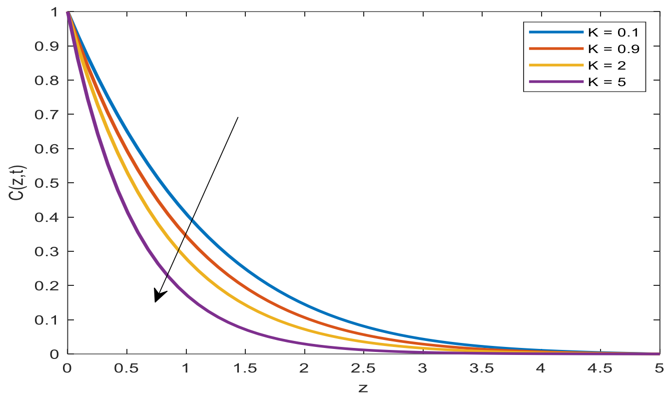

Fig. 6. Concentration for various values of chemical reaction parameter (K)

Figure 5 illustrates how concentration C varies with distance z for various Schmidt number (Sc) values. It has been shown that as (Sc) increases, the concentration profile decreases. (Sc) larger values equate to lower mass diffusivity. Lower mass diffusivity reduces species diffusion, giving a lower concentration boundary layer. Figure 6 depicts concentration distribution (C) against the distance z for different chemical reaction parameter (K) values. In all cases, the concentration falls with increasing z. The decrease is more pronounced for larger (K). This is because more intense chemical reactions improve the use of diffusing species and thus lead to a thinner concentration boundary layer

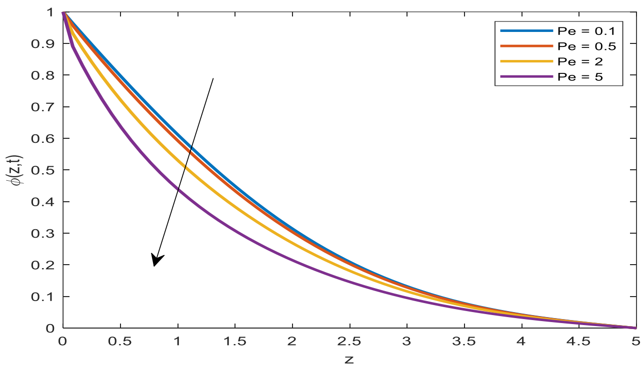

Fig. 7. Microorganism density profile for different values of Peclet number (Pe)

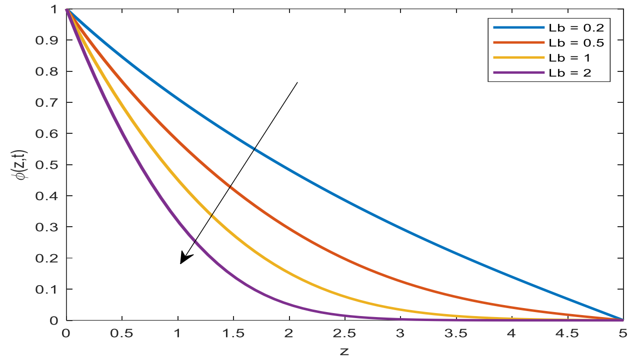

Fig. 8. Microorganism density profile for different values of bioconvection Lewis number (Lb)

Figure 7 illustrates the microorganism density profile for different "Peclet number (Pe)" values. Microorganism density falls as Pe rises because of less diffusion and increased convective movement. The microorganism boundary layer thins as a result. Microorganism density profile for various "bioconvection Lewis number (Lb)" values is shown in Figure 8. Because microbe diffusivity is decreased, it has been found that raising Lb lowers microorganism density. Therefore, the boundary layer's thickness reduces significantly.

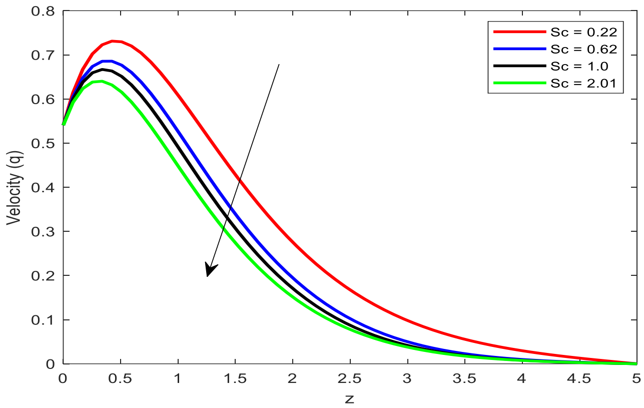

Fig. 9. Velocity profile for various values of (Sc)

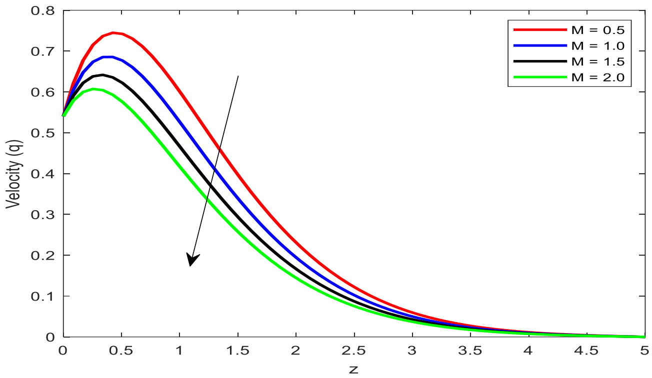

Fig. 10. Velocity profile for various values of (M)

The velocity profile for various Sc values is demonstrated in Figure 9. As Sc increases, fluid velocity falls. A greater Sc indicates a thinner momentum barrier layer and lower mass diffusivity, indicating less species mobility. For varied magnetic parameter (M) values, Figure 10 illustrates velocity circulation. As the magnetic parameter increases, the velocity profile decreases. Lorentz force of the applied magnetic field opposes fluid velocity and significantly reduces flow.

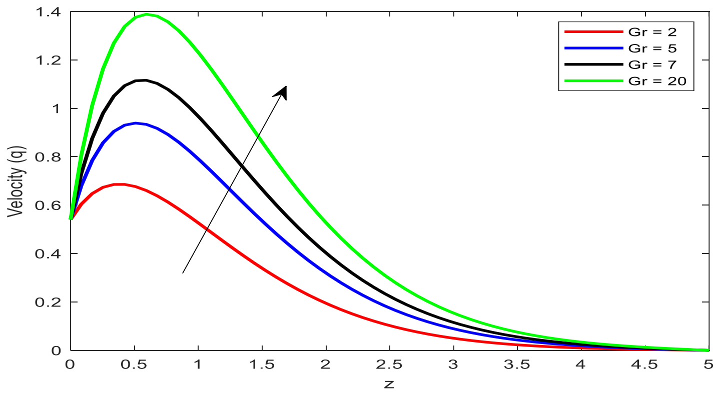

Fig. 11. Velocity profile for various values of (Gr)

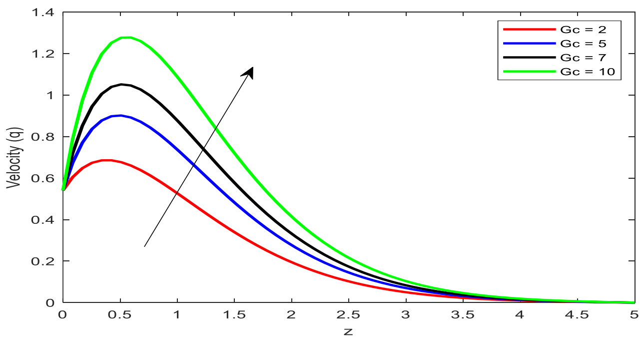

Fig. 12. Velocity profile for various values of (Gc)

Figures 11 and 12 demonstrate velocity profiles for different (Gr) and solutal Grashof number (Gc). In every image, velocity rises near the plate surface and decreases as z increases. The thermal buoyancy force is increased by higher values of Gr, while larger values of Gc enhance the buoyancy effect due to concentration differences. Thus, both values considerably increase the fluid velocity.

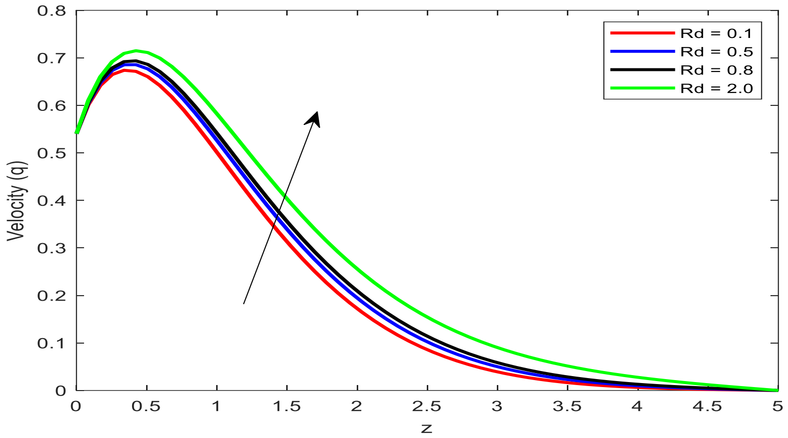

Fig. 13. Velocity profile for various values of (Rd)

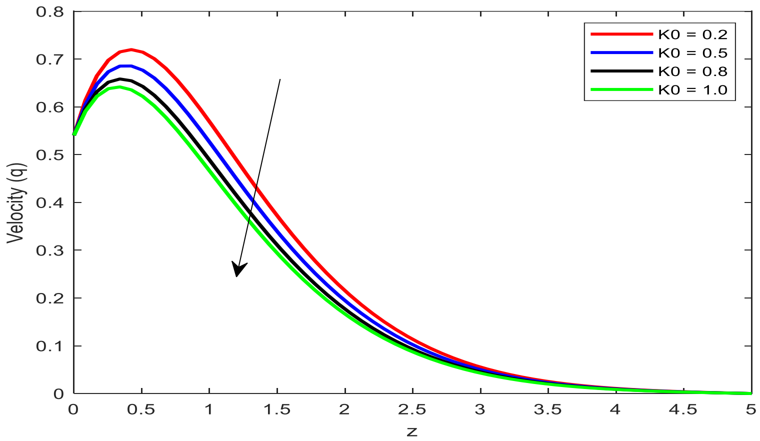

Fig. 14. Velocity profile for various values of (K0)

Figures 13 and 14 display the velocity variation for distinct settings of the radiation parameter (Rd) and permeability parameter (K0). The velocity increases as Rd increases, as shown in Figure 13. Thermal radiation increases fluid temperature, and buoyancy accelerates flow. In Fig. 14, the velocity drops with the increase of K0. This is because fluid motion slows down, and the momentum boundary layer decreases because of the porous medium's increased resistance.

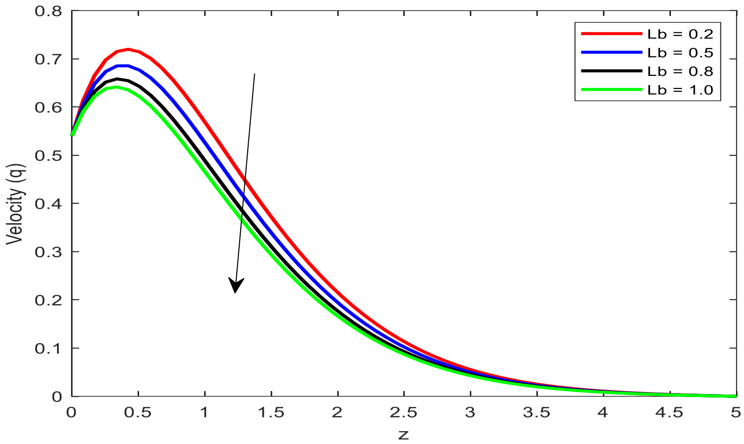

Fig. 15. Velocity profile for various values of (Lb)

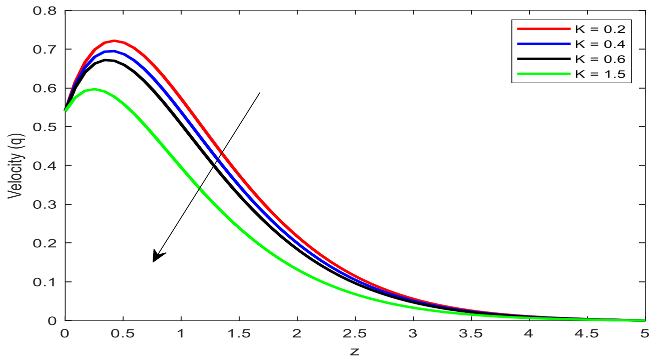

Fig. 16. Velocity profile for various values of (K)

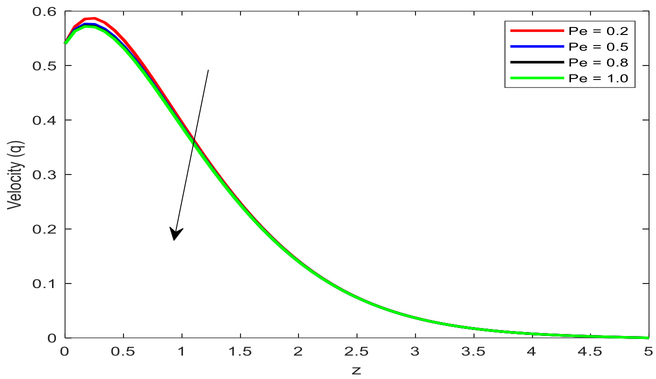

Fig. 17. Velocity profile for various values of (Pe)

Figures 15–17 depict velocity profiles for different values of bioconvection Lewis number (Lb), chemical reaction parameter (K), and Pe. As Lb increases, velocity decreases (Figure 15). This is because when Lb increases, microorganism diffusivity decreases, reducing bioconvection and fluid motion. The velocity falls with increasing K in Figure 16 because stronger chemical reactions lead to a decrease in species concentration and a weakening of the buoyant force. As seen in Figure 17, the velocity falls as Pe increases. This is because the stronger advective transport inhibits the microorganism diffusion, which reduces the strength of bioconvective flow.

V. Conclusions

The unsteady radiative magnetohydrodynamic bioconvective flow of a Fe_3O_4–MoS_2 hybrid nanofluid over a quickly inclined oscillating plate integrated in a rotating porous medium is the focus of this work. The current work's major contribution is the unification of the combined impacts of hybrid nanoparticles, heat radiation, magnetic effects, porous drag, system rotation, plate tilt, and microorganism-induced bioconvection in a single mathematical framework. MATLAB is employed to numerically solve the coupled nonlinear partial differential equations using the Crank-Nicolson finite difference method. The temperature field elevates with radiation and heat generation parameters but reduces with Pr, according to numerical results. The temperature field increases with increasing radiation and heat generation parameters, but it reduces with increasing Prandtl number, according to the numerical results. This suggests that the boundary layer region has inadequate species diffusion. Additionally, as the Schmidt number, Hartmann number, radiation parameter, and bioconvection Lb increase, the velocity profile decreases. On the contrary, velocity is greatly increased with the increasing Grashof number and Peclet number due to the higher buoyancy and microbe transport effects. Finally, the work emphasises the substantial impact of temperature, solutal, magnetic or bioconvective parameters on the transport behaviour of Fe_3O_4–MoS_2 hybrid nanofluid flow. The results are important insights for the development of new cooling technologies, biomedical transport systems, microbial fuel devices and industrial applications utilising hybrid nanofluids in rotating porous settings.

VI. Future Scope of the Study

There are various key extensions of the present study that can be made to increase its practical relevance and scientific contribution. Future research can include the introduction of non-Newtonian base fluids like Casson, Williamson, Carreau, or Maxwell fluids to better simulate industrial and biological liquids. Variable thermal conductivity, temperature-dependent viscosity, and nonlinear thermal radiation effects may also be introduced for more realistic thermal analysis. Further investigations can be performed on different combinations of nanoparticles and ternary hybrid nanofluids to compare the heat transfer efficiency of the present Fe_3O_4-MoS_2 “hybrid nanofluid.” Effect of slip boundary conditions, convective heating, Joule heating, viscous dissipation, and chemical reaction kinetics can also be examined. Moreover, the model can be generalised to 3-dimensional geometries, stretch/shrink of surfaces, curved channels or cylindrical domains, which would expand engineering applications.

VII. Limitations of the study

The present analysis is based on simplified assumptions such as laminar, incompressible, and one-dimensional flow conditions. The thermophysical parameters of the Fe_3O_4-MoS_2 hybrid nanofluid were assumed to be constant, omitting the effects of particle agglomeration and temperature dependence. The porous material and magnetic field were considered homogeneous and idealised. More importantly, the numerical conclusions derived by the Crank–Nicolson approach were not verified by experimental observations.

Conflict of Interest:

The authors declare that there was no relevant conflict of interest regarding this paper.

References

I. Aboel-Magd, Y., Basem, A., Farooq, U., Fatima, N., Noreen, S., Waqas, H., Iftikhar, M. (2024). "Computational modeling of thermal radiation and activation energy effects in Casson nanofluid flow with bioconvection and microorganisms over a disk." *International Journal of Thermofluids*, *23*, 100735. 10.1016/j.ijft.2024.100735

II. Asaigeethan, P., Loganathan, K., Karthik, V., Priyadharshini, D., & Arunachalam, K. P. (2025). "Microbiologically Induced Bioconvection Over a Convectively Heated Rotating Frame: A Computational Model of the Blood-Based MHD Casson Hybrid Nanofluid Flow." *International Journal of Thermofluids*, 101368.10.1016/j.ijft.2025.101368.

III. Almarashi, A. M., Algarni, A., Rooman, M., Shah, Z., & Garalleh, H. A. (2024). "Entropy generation and heat transfer analysis of unsteady micropolar magnetized hybrid-nanofluid flow over a radially stretchable permeable rotating disk with viscous and joule dissipation effects." *International Journal of Thermofluids*, *23*, 100802. 10.1016/j.ijft.2024.100802.

IV. Bijjula Prabhakar Ready and Oluwole D Makinde "Radiating and reacting unsteady MHD free Convection boundary layer flow past an oscillating vertical plate in a porous medium with Newtonian heating." International Journal of Applied Mechanics and Engineering, vol. 27(1), pp.168-187**,** 10.2478/ijame-2022-0011.

V. Choudhary, P., Loganathan, K., Jat, K., Sharma, K., & Eswaramoorthi, S. (2025). "Shape factor analysis of water and aluminium oxide nanoparticles in a porous medium with slip effects." *Chemical Physics Impact*, *10*, 100882.10.1016/j.chphi.2025.100882

VI. Choudhary, P., Choudhary, S., Jat, K., Loganathan, K., & Eswaramoorthi, S. (2024)."Impacts of unsteady MHD hybrid nanofluid over a non-linear stretchable porous sheet with thermal radiation and gyrotatic microorganisms." *International Journal of Thermofluids*, *23*, 100788. 10.1016/j.ijft.2024.100788.

VII. Choudhary, S., Kumar Jarwal, V., Choudhary, P., Loganathan, K., & Pattanaik, B. (2024). "Mass-Based Hybrid Nanofluid Model for Thermal Radiation Analysis of MHD Flow over a Wedge Embedded in Porous Medium." *Journal of Engineering*, *2024*(1), 9528362. 10.1155/2024/9528362.

VIII. Choudhary, R., Parmar, A., Kumar, P., & Al-Mdallal, Q. (2025). "Buoyancy effects on Falkner-Skan Maxwellian nanofluid flow with bioconvection over a melting wedge." *International Journal of Thermofluids*, *26*, 101136. 10.1016/j.ijft.2025.101136.

IX. Choudhary, P., Choudhary, S., Jat, K., Loganathan, K., & Eswaramoorthi, S. (2024). "Significance of melting heat transfer and bioconvection phenomena in nanofluid flow over three different geometries." *International Journal of Thermofluids*, *24*, 100855. 10.1016/j.ijft.2024.100855

X. Choudhary, P., Loganathan, K., Jat, K., Arunachalam, K. P., & Eswaramoorthi, S. (2025). "Thermal and velocity slip impacts on MHD tetra-hybrid nanofluids flow over a porous stretching surface." *Discover Applied Sciences*, *7*(7), 720. 10.1007/s42452-025-07359-6.

XI. Kavitha, S., and Ayothi Selvaraj. (2024). "Rotation and Dufour Impact on Unsteady Flow Past a Parabolic Accelerated Vertical Plate with Uniform Temperature and Mass Diffusion." *Indian Journal of Science and Technology* 17 (24): 2482–2493. 10.17485/IJST/v17i24.1422

XII. Lakshmikaanth, D., Selvaraj, A., Selvaraju, P., & Jose, S. D. (2023). "Hall and heat source effects of flow past a parabolic accelerated isothermal vertical plate in the presence of chemical reaction and radiation." *JP Journal of Heat and Mass Transfer*, *34*, 105-126. 10.17654/0973576323035

XIII. Lakshmikaanth, D., Selvaraj, A., Tamilselvi, L., Jose, S. D., & Velukumar, V. (2024). "Hall and heat source effects of flow state on a vertically accelerating plate in an isothermal environment, including chemical reactions, rotation, radiation, and the Dufour effect." *JP Journal of Heat and Mass Transfer*, *37*(4), 491-520. 10.17654/0973576324034.

XIV. Prabhakar Reddy, B., & Makinde, O. D. (2022). "Numerical study on MHD radiating and reacting unsteady slip flow past a vertical permeable plate in a porous medium." *International Journal of Ambient Energy*, *43*(1), 6007-6016.10.1080/01430750.2021.1999323.

XV. Prabhakar Reddy B, Simba M. H, and Alfred Hugo. "Effects of thermo-diffusion and chemical reaction on MHD radiated unsteady flow past an exponentially accelerated inclined permeable plate embedded in a porous medium. "International Journal of Chemical Engineering**,** 10.1155/2023/9342174

XVI. Prakash, J., Selvaraj, A., Ragupathi, P., Al-Mdallal, Q. M., & Saranya, S (2025). "Thermal and radiative effects on unsteady MHD flow of Casson fluid past a rotating porous medium with variable mass diffusion." Case Studies in Thermal Engineering, 68, 105865. 10.1016/j.csite.2025.105865.

XVII. Radha, Ganesan, Ayothi Selvaraj, Neel Armstrong Abraham, Sundar Rajan Deepa, Mani Lakshmi, and Devi Lakshmikaanth (2025). "First Order Chemical Reaction Effects on Unsteady MHD Casson Fluid Flow Past a Parabolic Accelerated Vertical Plate with Uniform Mass Diffusion and Variable Temperature in the Presence of Thermal Radiation." *Journal of Advanced Research in Fluid Mechanics and Thermal Sciences* 133 (1): 24–36. 10.37934/arfmts.133.1.2436

XVIII. Rajakumar, K.V.B., K.S. Balamurugan, M. Umasankara Reddy, and Ch. V. Ramana Murthy(2018). "Radiation, Dissipation and Dufour Effects on MHD Free Convection Casson Fluid Flow through a Vertical Oscillatory Porous Plate with Ion-Slip Current." International Journal of Heat and Technology 36 494–508. 10.18280/ijht.360214.

XIX. Rajakumar, K. V. B., Govinda Rao, T., Umasankara Reddy, M., & Balamurugan, K. S. (2020). "Influence of Dufour and thermal radiation on unsteady MHD Walter's liquid model-B flow past an impulsively started infinite vertical plate embedded in a porous medium with chemical reaction, Hall and ion slip current." *SN Applied Sciences*, *2*(4), 742. 10.1007/s42452-020-2484-y

XX. Rao, Shiva, and P. N. Deka.(2024) "Numerical Analysis of MHD Hybrid Nanofluid Flow a Porous Stretching Sheet with Thermal Radiation." International Journal of Applied and Computational Mathematics, 10(3). 10.1007/s40819-024-01734-4.

XXI. Raju, R., Selvaraj, A., Jose, S. D., & Chithra, K. (2025). "Effects of radiation and heat generation on MHD Casson fluid flowing in a porous medium rotating on an inclined oscillating vertical plate." *JP Journal of Heat and Mass Transfer*, *38*(3), 315-339. 10.17654/0973576325016

XXII. Reddy, B. P. (2020). "THERMO—diffusion and HALL effect on radiating and reacting MHD convective heat absorbing fluid past an exponentially accelerated vertical porous plate with ramped temperature." *Journal of the Serbian Society for Computational Mechanics*, *14*(1), 12-28. 10.24874/jsscm. 2020.14.01.02

XXIII. Radha, Ganesan, Ayothi Selvaraj, Soundararajan Bhavani, and Periasamy Selvaraju, Magneto Hydrodynamic Effects on Unsteady Free Convection Casson Fluid Flow Past on Parabolic Accelerated Vertical Plate with Thermal Diffusion, Journal of Advanced Research in Fluid Mechanics and Thermal Sciences. 116(1) (2024) 184-200. 10.37934/arfmts.116.1.184200

XXIV. Selvaraj, A., and E. Jothi(2021). "Heat Source Impact on MHD and Radiation Absorption Fluid Flow Past an Exponentially Accelerated Vertical Plate with Exponentially Variable Temperature and Mass Diffusion through a Porous Medium."Materials Today: Proceedings 46 (2021): 3490–94. 10.1016/j.matpr.2020.11.919

XXV. Selvaraj, A., Aruna, M., Deepa, S., Dilip Jose, S., Dhas, S. S. J., & Alotaibi, M. T. (2025). "Harnessing of potential Hall and Dufour Effects on MHD flow over a parabolically accelerated vertical plate." *ZAMM-Journal of Applied Mathematics and Mechanics/Zeitschrift für Angewandte Mathematik und Mechanik*, *105*(11), e70288. 10.1002/zamm. 70288.

XXVI. Sebastian, Dilip Jose, Mercy S. Fayemi, and Ayothi Selvaraj. 2024. "Unravelling the Complexities of Thermal Radiation and Rotational Dynamics in Parabolic Flow: A Perspective." *JP Journal of Heat and Mass Transfer*

XXVII. Vijayaragavan, R., M. Ramesh, and S. Karthikeyan, Heat and Mass Transfer Investigation on MHD Casson Fluid Flow past an Inclined Porous Plate in the Effects of Dufour and Chemical Reaction, Journal of Xi'an University of Architecture and Technology. 13 (2021) 860-873. 10.37896/JXAT13.6/31183